Desalination and Water Treatment
www.deswater.com

doi: 10.5004/dwt.2020.25842

194 (2020) 160–171
August

The capability of nano-scale zero valent iron particles for removal of concentrated lead in spent acidic regeneration solution

Surapol Padungthon[a,b], Antika Pranudta[a], Medhat Mohamed El-Moselhy[c], Pinit Kidkhunthod[d], Penphitcha Amonpattaratkit[d], Pijit Jiemvarangkul[e,*]

[a]*Department of Environmental Engineering, Khon Kaen University, Khon Kaen 40002, Thailand*
[b]*Advanced Functional Nanomaterials and Membrane for Environmental Remediation (AFMFR) Laboratory, Khon Kaen University, Khon Kaen 40002, Thailand*
[c]*Department of Chemistry, Faculty of Science, Al-Azhar University, 11884 Nasr City, Cairo, Egypt*
[d]*Synchrotron Light Research Institute, 111 University Avenue, Muang District, Nakhon Ratchasima 30000, Thailand*
[e]*Department of Civil Engineering, King Mongkut's University of Technology North Bangkok, Bangkok 10800, Thailand, email: pijit.j@eng.kmutnb.ac.th (P. Jiemvarangkul)*

Received 23 September 2019; Accepted 16 March 2020

ABSTRACT

Nano zero-valent iron particle (nZVI) is a type of nanoparticles, which can eliminate several pollutants in water including heavy metal contamination in both groundwater and industrial wastewater. This research was created to examine the capability of nano zero-valent iron particles to remove very high Pb^{2+} concentration in spent regeneration solution (100 – 3,000 mg/L). At Pb^{2+} concentrations <1,000 mg/L, nZVI particles can remove lead up to 99% within 30 min. Compared with micro zero-valent iron powder, nZVI has lead removal efficiency 12–20 times higher than those of micro zero-valent iron. Adsorption isotherms (Langmuir and Freundlich models) were used to present the monolayer adsorbed and chemisorption process of adsorbed lead on surface of nZVI particles with maximum adsorption capacity was 1,666 mg-Pb/g-nZVI. Adsorption occurred was a pseudo-second-order reaction with the correlation between rate constant and initial concentration of Pb^{2+}. Elemental analysis obviously found lead accumulated on the surface of nZVI particles. From X-ray absorption fine structure study, Pb atoms can adsorb onto the surface ferric oxide through the formation of the inner-sphere complex with the distance between Fe and Pb atoms approximately 3.67 Å.

Keywords: Adsorption rate; Nanotechnology; Redox reaction; nZVI; Isotherm; Kinetics; Pb^{2+}

1. Introduction

Nanoscale zero-valent iron particles (nZVI) have been in focus in research for more than 20 y and have been used for environmental clean-up, especially hazardous waste since 2000 [1–4]. The nZVI with huge surface areas is a powerful reducing agent with an adsorption property to rapid uptake and transform many environmental contaminants. The nZVI treating polychlorinated hydrocarbon has been the focusing research literatures at the earlier stage of nZVI study. Several lines of evidence have revealed that nZVI can reduce a number of hazardous chemical agents such as heavy metal ions, perchlorate, nitrate, polychlorinated biphenyls (PCBs), chlorinated solvents, organochlorine pesticides, and organic dyes, effectively [2,5–13]. Due to the shape of nZVI that can be transported by pumping and can be directly injected to the source of contamination underground and with its significantly high

* Corresponding author.

reactive, nZVI is more extensively used *in situ* remediation. There are more than 10 remediation fields using nZVI and bimetallic nZVI to treat trichloroethylene (TCE) in USA [14]. Mixed nZVI with micro-ZVI was used to treat PCE contaminated site in Bornheim, Germany. The remediation was able to reduce the predicted treatment time from 50 y down to 2 y with a 90% reduction of total contaminated chlorinated compounds with no byproducts increasing [15]. There are other two *in situ* remediations of chlorinated hydrocarbon in the Czech Republic that were reported of successfully reducing contamination by using nZVI [15].

Not only chlorinated hydrocarbon is identified as environmental contamination, but also heavy metal ions are one of the most toxic pollutants especially contaminated in water. They are released to water resources from natural weathering processes, mines, and industrials. One of the concern metal ions is Lead, Pb^{2+}, which is one of the most important metals for industrials. It has been used in several manufacturing such as battery manufacturing, painting pigment, fuel, automobile, etc. [16,17]. Pb^{2+} is very toxic to living being and can be accumulated in animal or human tissues [18]. Chemical co-precipitation such as alum or ferric chloride is one of the conventional methods for removal of lead from industrial wastewater. However, voluminous hazardous waste sludge can add the treatment cost for the whole system. Note that nowadays, many various industrial-grade regenerable adsorbents, for example, chelation resins are gaining popularity and finally adopt for removal of lead-contaminated in wastewater due to save chemical adjustment cost, possible for recycled treated acidic water [19,20]. After the service run, there are only a small volume of spent regeneration waste approximately five-bed volumes. Therefore, it is very important to remove it from wastewater before disposal. Since the spent regeneration waste contains medium acidic (pH 3) with high concentration of heavy metals, that is, Pb^{2+} elutes out of the material, the application of nZVI can be one of the promising methods. From the literature review, there are limited studies so far about the application of nZVI for the treatment of high concentration heavy metal (Pb^{2+}) in spent acidic waste from regeneration.

Recent studies have indicated that nZVI is one of the adsorbents, which is a strong reducing agent and has adsorption ability with many advantages to treat water contaminated by heavy metals [2,17,21,22]. The nZVI has been found to be used to successfully removal various heavy metal ions such as Co^{2+}, Cu^{2+}, Pb^{2+}, Ba^{2+}, As^{3+}, As^{5+}, and Cr^{6+} in solutions [7,21,23–25]. Boparai et al. [26] showed the ability of nZVI to adsorb Cd^{2+} for aqueous solution with the adsorption capacity at 769.2 mg/g at 297 K. Moreover, nZVI has been used as composite materials to remove heavy metals in aqueous solution such as nZVI-graphene composite to Co^{2+} adsorption, zeolite-nZVI composite to removal Pb^{2+} [27], and hybrid cation gel exchanger containing nZVI particles to remove Pb^{2+} [19]. Based upon those discovers, nZVI is one of potential materials that can be developed for using to treating heavy metal, especially Pb^{2+} in industrial waste treatment. To use it in that propose, we need the basic properties of pure nZVI, such as adsorption isotherm and mechanism, reaction kinetic parameters, etc. However, few data have reported on pure nZVI properties in Pb^{2+} adsorption and reaction. The aims of this work were set up to determine the maximum ability of nZVI to remove lead contaminated in synthetic wastewater and to provide the kinetic and adsorption parameters of the Pb-nZVI reactions for engineering applications in future use of nZVI.

2. Materials and methods

2.1. Chemicals and materials

Ferric chloride ($FeCl_3$) was obtained from Alfa Aesar (UK). HCl (12.1 N) and HNO_3 (15.8 N) were used. Ninety eight percent purity of sodium borohydride ($NaBH_4$) was used in this work. Pentane 99%, spectrophotometric grade was obtained from Sigma-Aldrich (USA). Ninety five percent of ethanol was purchased from Pharmco-Aaper (USA).

2.2. nZVI synthesis

In this research, nZVI was synthesized by reacting ferric chloride solution with sodium borohydride solution. 0.18 M $FeCl_3$ and 0.94 M $NaBH_4$ at 1:1 volume ratio was added, then were rapidly mixed in a batch reactor with stirring speed higher than 400 rpm. The reaction to produce zero-valent iron was shown as follow:

$$4Fe^{3+}_{(aq)} + 3BH^{-}_{4(aq)} + 9H_2O \rightarrow 4Fe^{0}_{(s)} + 3H_2BO^{-}_{3(aq)} + 12H^{+}_{(aq)} + 6H_{2(g)} \quad (1)$$

Iron nanoparticles were formed and collected by filtrating through 0.2 μm filter papers. Then, collected nZVI were washed by ethanol solution. Scanning electron microscopy (SEM) was used to detect the average size of nZVI (about 60–70 nm) [28,29]. The collected nanoparticles were kept in a sealed polyethylene container under ethanol solution and put in a refrigerator. The moisture content of nZVI samples was averagely 70%. In this study, the particles were used within 1 d after synthesized.

2.3. Adsorption and kinetic experiments

Adsorption isotherms and kinetics were determined by varying initial Pb^{2+} concentrations from 100 to 3,000 mg/L in 100 mL solution with 0.5 g nZVI in 200 mL flask sealed by parafilm. The samples were collected during 0–180 min to quantify the Pb^{2+} concentration. The Pb^{2+} concentration in aqueous solution was measured by inductively coupled plasma-atomic emission spectrophotometer.

2.4. Electron microscope

The SEM (Hitachi 4300, Japan) was used to detect the morphology of nZVI. The character of nanomaterials was shown in 3D topographical images by secondary electron (SE) imaging mode, and an energy-dispersive X-ray spectrometer was used to quantify the elemental mapping of nZVI particles [30]. Imaging under SE mode was typically conducted at 5 kV accelerating voltage. nZVI particle specimens were coated with a thin layer of iridium to reduce surface charging. Transmission electron microscopy (TEM) was used

to take TEM images of nZVI particle samples. Two to three droplets of nZVI particle specimens suspended in ethanol solution were dropped onto a holey carbon film and were dried before TEM imaging process.

2.5. X-ray absorption spectroscopy data collection and analysis

The Fe *K*-edge were collected at beamline BL 5.2 – SUT-NANOTEC-SLRI XAS (X-ray absorption spectroscopy) of the Synchrotron Light Research Institute (SLRI), Thailand. The synchrotron ring was operated at 1.2 GeV and at currents between 100 and 150 mA. The reaction cell was mounted onto a sample holder and placed in a He-filled chamber. The Ge (220) double-crystal monochromator with an energy resolution ($\Delta E/E$) of 2×10^{-4} was used to scan the synchrotron X-ray beam which was calibrated using an elemental Fe foil reference sample (7,112 eV). The XAS spectra (X-ray absorption near edge structure (XANES) and extended X-ray absorption fine structure (EXAFS)) of Fe *K*-edge in Fe reference samples, new-nZVI, and nZVI adsorbed Pb (Pb-nZVI) were measured in transmission mode. The spectra of Pb L_3-edges (13,035 eV) XANES measurements were conducted at beamline BL 8 – XAS of SLRI. All samples were conducted at room temperature using a Ge (220) double-crystal monochromator. Pb foil and PbO were used for standard and recorded in the transmission mode, while the Pb-nZVI sample were obtained in the fluorescence mode with a 13-element Ge detector. All data of XAS were fitted by non-linear least-square methods using IFFEFIT software package [19].

3. Results and discussion

3.1. nZVI properties

Synthesized nZVI particles are black color sludge and black powder after dried. When adding 0.5 g of nZVI into 100 mL of deionized water (DI water), average pH of the solution is around 7.8 and the moisture of harvested nZVI is around 70%. Moisture content of nZVI was measured by detecting particles weight before and after typically drying particles in 103°C oven for 24 h and let them cool down at room temperature. SEM revealed the cluster of small particles and TEM presented the chain-like cluster of nanoscale particles as shown in Fig. 1. From TEM image (Fig. 1b), most of the small particles have their diameter less than 100 nm. From the properties detected, nZVI used in this work was similar to typical nZVI particles used in several researches, which produced the particles in the same method.

3.2. Scanning electron microscopy–energy-dispersive X-ray spectroscopy analysis

After reacting with Pb^{2+}, the physical body of particles was changed from almost round shape to sponge-like shape of thick shell as shown in Fig. 2a. The surface of reacted particles was rough and covered by thick porous layer, which contained of oxide of iron, and some of particles lose their zero-valent iron core due to the oxidation of iron with surrounding environment, for example, water and Pb^{2+}. EDS results illustrated the appearance of Pb element on the surface of nZVI particles as represented in Figs. 2b and c. The EDS spectrum provided the characteristic peaks for Pb at around 2.5 keV for electron transmission to M shell and 10–15 keV for electron transmission to L shell. The ratio of Pb on particle surface was increased from 5% to almost 35% when increasing concentration of Pb^{2+} in solution. The EDS results suggested the binding of lead ions onto the nZVI surface. Moreover, there are researches confirming that the both reduction and adsorption are the removal mechanism of Pb^{2+} removal from aqua solution [17,31]. The XANES and EXAFS characterization will be further used to elucidate the Pb^{2+} removal mechanism by nZVI.

3.3. Pb^{2+} removal efficiency

The experiments were set up by mixing 0.5 g dry of nZVI with various concentrations of 100 mL Pb^{2+} solution

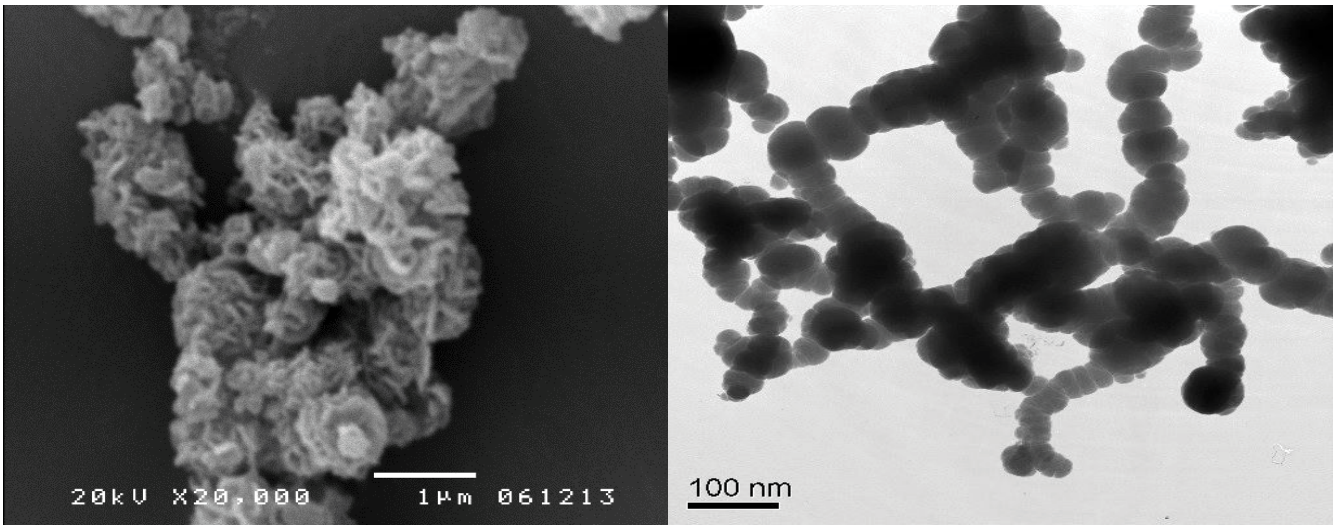

Fig. 1. Electron microscope images of nZVI (a) SEM and (b) TEM.

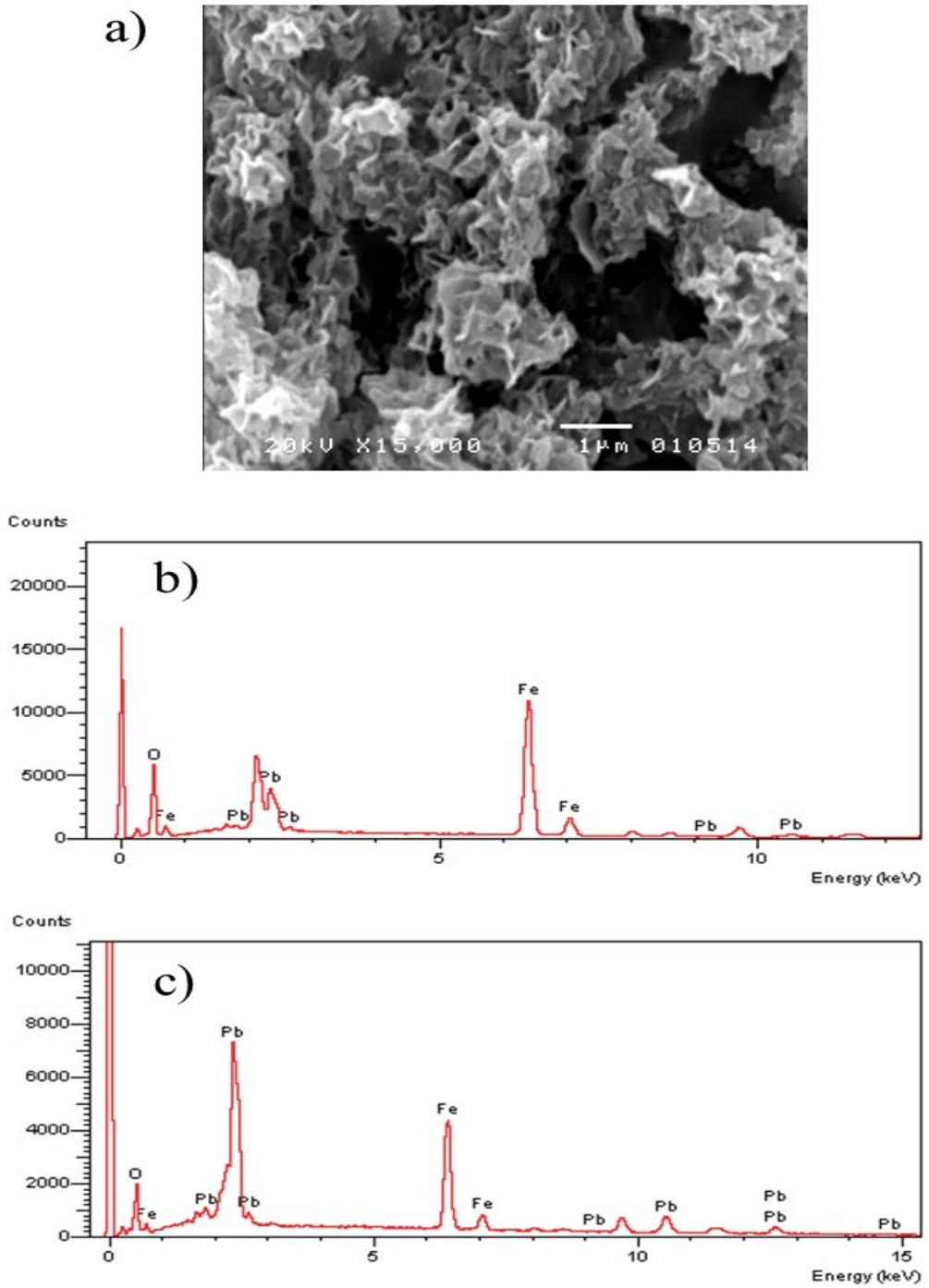

Fig. 2. Physical images of nZVI particles and EDS results (a) after reacting with 3,000 mg/L of Pb^{2+} for 180 min, (b) at 500 mg/Lof Pb^{2+}, and (c) at 3,000 mg/L of Pb^{2+}.

(100–3,000 mg/L) for 180 min. The pH of Pb^{2+} solutions before adding nZVI were ranged from 4.3 to 5.2. The results showed that the rapid decrease of Pb^{2+} in solution within 10 min at low concentration (<1,000 mg/L) samples and the Pb^{2+} removal was still continuous until the end of experiment at 180 min as shown in Fig. 3a. The removal efficiency of all experiments was presented in Fig. 3b. In cases of low concentration samples (<1,000 mg/L), more than 80% of lead was removed within 10 min and nearby 100% removal (>99%) at 180 min mixing time. At high concentration samples (1,000–3,000 mg/L), the results showed that Pb^{2+} was considerably decreased within 30 min and gradually decreased after 60 min (Fig. 3a).

The removal efficiency after 180 min of 1,000 and 3,000 mg/L samples was 90.6% and 67.3% (Fig. 3b) indicting that removal efficiency was reduced when the initial

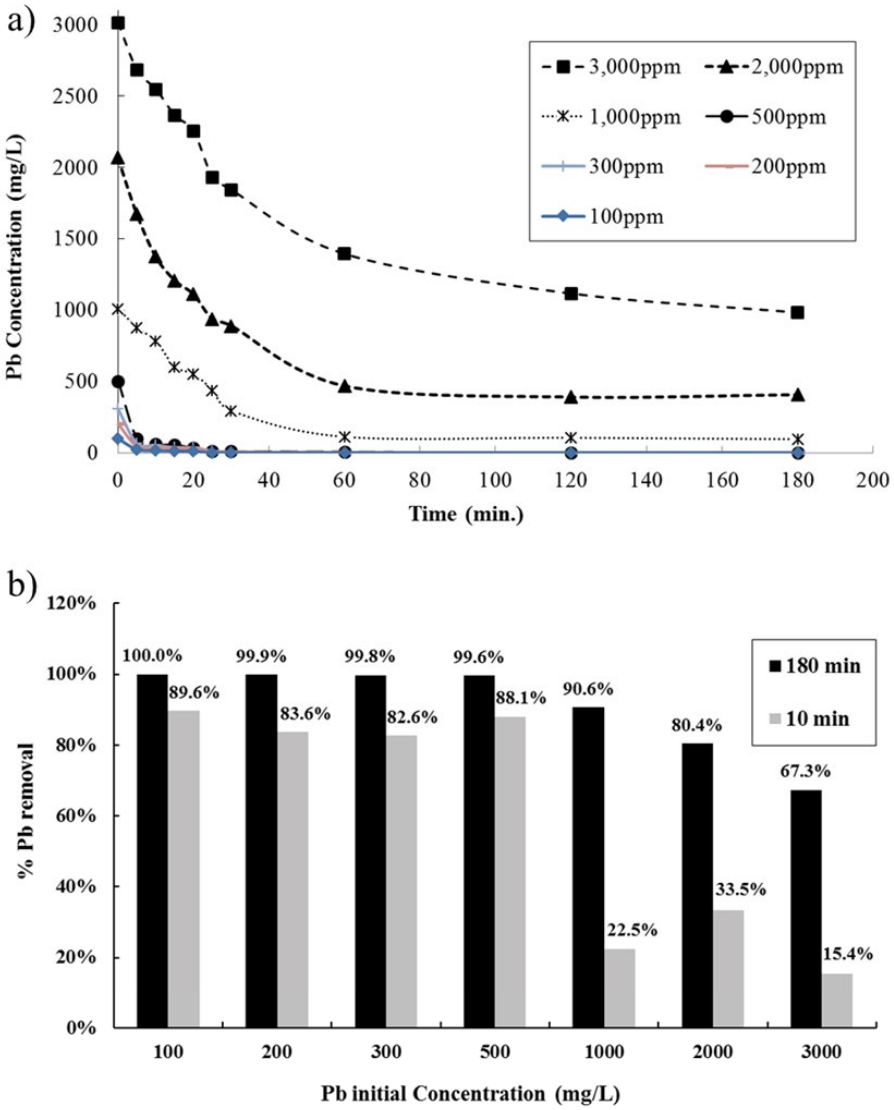

Fig. 3. Lead (Pb) removal by 0.5 g of nZVI (a) at various Pb initial concentrations and (b) removal efficiency at 10 and 180 min reaction times.

concentration of Pb^{2+} increased. Moreover, average pH of all samples after reaction was around 8.2 due to H^+. Micro Fe particles were only able to remove 5%–10% of Pb^{2+} at sample concentration of 200–500 mg/L (data not shown) at the similar reaction time (180 min). The comparison between nanoscale and micro size of Fe particles showed significant different removal efficiency for Pb^{2+}. From the removal results, mass of Pb^{2+} adsorbed on nZVI particles, q (mg/g nZVI), was calculated and shown in Fig. 4. At concentration lower than 500 mg/L, the results showed that adsorption process reached to equilibrium within 30 min (actually within 10 min). The adsorption process of 500 mg/L and higher concentrations showed the equilibrium after 60 min. Only 3,000 mg/L of lead, the process still continuously progressed even after 180 min. The results suggested the very fast removal activity of Pb^{2+} by nZVI just in minutes. This ability of them can be developed to use for removal process in high concentration of Pb^{2+} contaminated wastewater.

3.4. Adsorption kinetic

The kinetics of the adsorption results were evaluated and interpreted by using the pseudo-first-order and pseudo-second-order models. Pseudo-first-order kinetics equation in linearized form is:

$$\log\left(q_e - q_t\right) = \log q_e - \frac{k_1}{2.303}t \tag{2}$$

where q_e and q_t (mg/g) are mass of Pb^{2+} adsorbed on nZVI particles (mg/g nZVI) at equilibrium and at time t (min) and k_1 is the pseudo-first-order rate constant (h^{-1}) of adsorption reaction [32]. The plots of $\log(q_e - q_t)$ vs. time was shown in Fig. 5a. k_1 and q_e at each experimental concentration of lead were calculated from Fig. 4 and shown in Table 1. The trend lines in Fig. 4a suggested that pseudo-first-order kinetics model was unfitting and R_1-square of each tread line was low

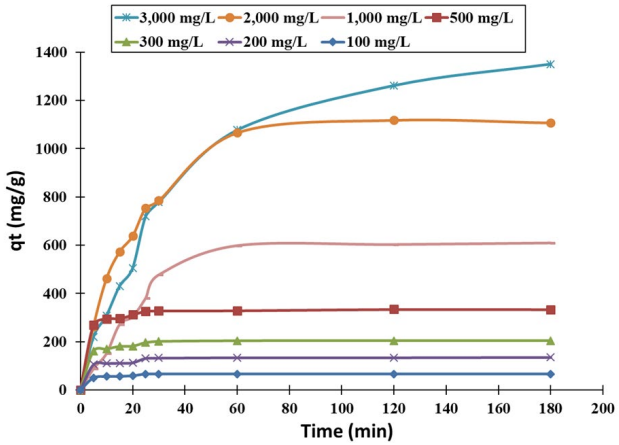

Fig. 4. Mass of lead adsorbed on nZVI particles (*qt*) in different reaction times.

as shown in Table 1. These results suggested that the pseudo-first-order kinetic model was not suited for the adsorption of Pb^{2+} on nZVI.

Pseudo-second-order kinetics equation for examining chemisorption kinetics [33] in linearized form is:

$$\frac{t}{q_t} = \frac{1}{k_2 q_e^2} + \frac{1}{q_e} t \tag{3}$$

where k_2 is the rate constant for pseudo-second-order adsorption (g/mg/h). Pseudo-second-order kinetics were performed by the plots of t/q_t vs. t (Fig. 5b). k_2 and q_e at each experimental concentration of Pb^{2+} were calculated from Fig. 4 and shown in Table 1. Fig. 5b showed almost perfectly fit to liner plots with the correlation coefficients (R^2) closing to 1.00 (>0.950). This result suggested that Pb^{2+} adsorption by nZVI follows pseudo-second-order kinetic. Therefore, Pb^{2+} adsorbed by nZVI particles was the chemical interaction phenomena [26,32]. There are several reports describing the relationship between k_2 and initial concentration of solute [32]. The calculated k_2 results (Table 1.) were plotted with Pb^{2+} initial concentration (C_0) as illustrated in Fig. 6. The relationship was clearly presented by the equation of $k_2 = 63.841 C_0^{-1.909}$ with R_2^2 of 0.9622. This suggested the strong relationship between kinetic constant k_2 with

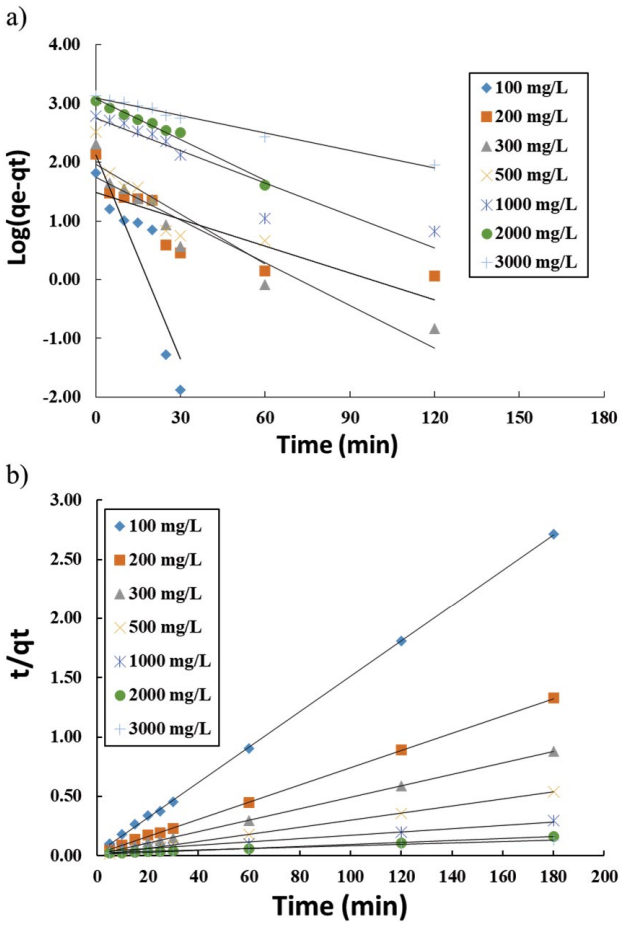

Fig. 5. Kinetic model plot for Pb^{2+} reacting with nZVI particles (a) pseudo-first-order and (b) pseudo-second-order kinetic.

initial concentration of Pb^{2+} in this case and therefore, the equation might be used to develop the use of nZVI to treat Pb^{2+} in environmental and industrial wastewater treatment application for the future.

3.5. Adsorption mechanism

The adsorption mechanism can be explained by Weber and Morris's intraparticle diffusion model (IPD). The

Table 1
Rate constants of adsorption kinetic model

Concentration (mg/L)	$q_{e,exp}$ (mg/g)	Pseudo-second-order			Pseudo-first-order		
		k_2 (g/mg/min)	$q_{e,cal}$ (mg/g)	R_2^2	k_1 (1/min)	$q_{e,cal}$ (mg/g)	R_1^2
100	66.37	0.0089	67.11	0.999	0.267	132.80	0.813
200	132.93	0.0031	136.99	0.999	0.035	30.31	0.648
300	203.15	0.002	208.33	0.999	0.056	55.92	0.888
500	328.22	0.0003	333.33	0.999	0.065	93.52	0.713
1,000	598.2	5.44E-05	714.29	0.979	0.042	562.73	0.888
2,000	1,066.6	5.05E-05	1,250.00	0.996	0.053	1,212.27	0.978
3,000	1,077.4	1.64E-05	1,666.67	0.992	0.023	1,246.81	0.989

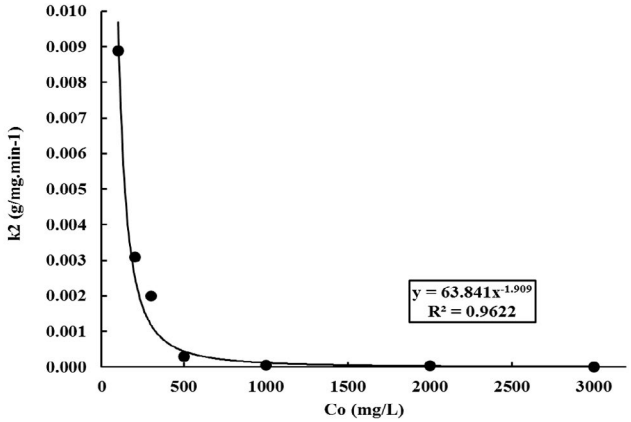

Fig. 6. Plot of apparent pseudo-second-order rate constant (k_2) vs. initial concentration (mg/L).

adsorption mechanism can be explained by three steps [26]. First step is surface diffusion, where the solute is moved from the solution to the outside surface of adsorbent. Second step is IPD, in which the solute molecules travel into the inside of sorbent particles. The final step is the equilibrium step. The molecules travel gradually deep from large pores into smaller pores causing a slow adsorption rate. The Weber–Morris IPD model is frequently been used to explain the IPD as the adsorption rate-limiting step [34–36]. The IPD equation is:

$$q_t = k_i t^{0.5} + C \tag{4}$$

where k_i is the IPD rate constant (mg g^{-1} min$^{0.5}$) and C is the intercept.

The plot of q_t vs. $t^{0.5}$ was shown in Fig. 7. Multi-linearity of the results presented two or three steps involving in the adsorption mechanism of lead onto the surface of nZVI particles. At low lead initial concentrations below 1,000 mg/L, rapid adsorption occurred due to a lot of unoccupied surface of nZVI particles. These can be observed by the intercept of the plots (Fig. 7a). This suggest that surface adsorption was occurred immediately and followed by intrapaticle diffusion. Therefore, the IPD was not the only rate-limiting mechanism at low concentration of Pb^{2+}. On the other hand, at high lead initial concentrations higher than 1,000 mg/L, the plots revealed multi-linear started from the line that passed through the origin (Fig. 7b). This indicated that IPD has role in the adsorption mechanism due to huge amount of adsorbates but limiting of adsorbent surface. The results suggested that the adsorption mechanism was controlled by IPD until reaching to equilibrium state [36]. At lead concentration of 1,000 mg/L, the plot showed the transition state of IPD model (Fig. 7b) [26,36]. Based on all results in Fig. 7, the IPD also played the important role for the adsorption of Pb^{2+} with nZVI.

3.6. Adsorption isotherms

Adsorption of Pb^{2+} by nZVI was investigated by Langmuir and Fruendlich isotherms. Langmuir isotherm assumption is

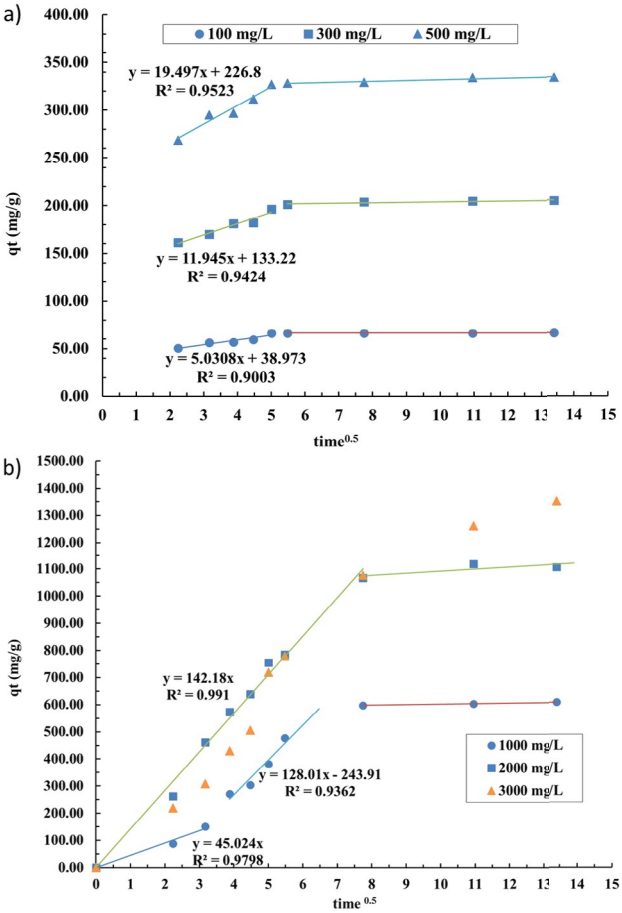

Fig. 7. Adsorption mechanism of Pb^{2+} with nZVI particles (a) concentration of Pb at 100, 300, and 500 mg/L (b) concentration of Pb at 1,000, 2,000, and 3,000 mg/L.

based on the adsorption of sorbate molecule on the surface of sorbent in monolayer with a limited surface of sorbent. The Langmuir model in linearized form is:

$$\frac{C_e}{q_e} = \frac{1}{K_L q_m} + \frac{C_e}{q_m} \tag{5}$$

where q_e is the mass of sorbate adsorbed per mass of adsorbent (mg/g) and C_e is the equilibrium concentration of sorbate (mg/L). The constants K_L is the Langmuir constant and q_m is the maximum adsorption capacity (mg/g) [26,37,38]. The straight tread line of a plot between C_e/q_e and C_e will give a slope of $1/q_m$ and an intercept of $1/q_m K_L$.The Langmuir isotherm was performed by the plots of C_e/q_e vs. C_e, at different concentrations, which were used to calculate q_m and K_L (Fig. 8a). Langmuir isotherm parameters were shown in Table 2. The plot of Langmuir isotherm (Fig. 8a) showed good agreement with observed behavior (R^2 > 0.95). The maximum adsorption capacity at room temperature (around 297–298 K) was 1,666.67 mg/g as shown in Table 2. The adsorption capacity as mole of adsorpbate per mole adsorbent was calculated as 0.45 mol/mol referring that two atoms of iron can catch one atom of lead.

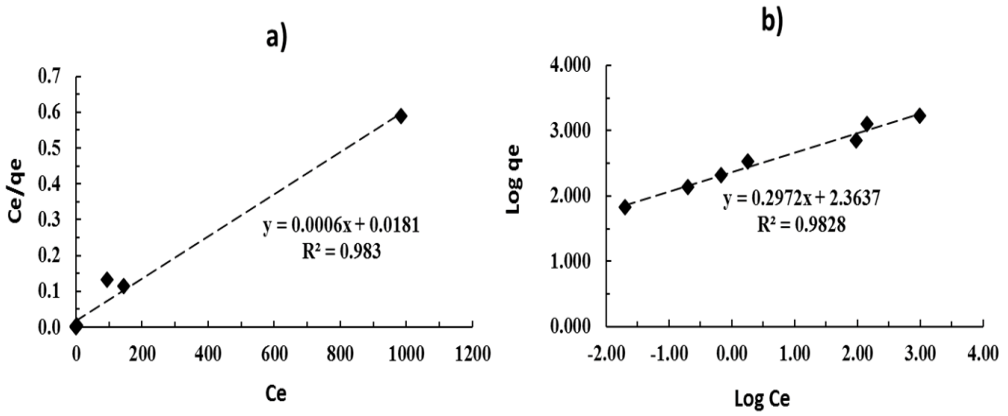

Fig. 8. Adsorption isotherms of Pb^{2+} with nZVI (a) Langmuir and (b) Fruendlich model.

Table 2
Adsorption isotherm model parameters

Langmuir isotherm			Freundlich isotherm			
K_L (L/mg)	q_m (mg/g)	R^2	K_F (L/g)	1/n	n	R^2
0.033	1,666.7	0.98	231.0	0.30	3.36	0.98

The Freundlich isotherm is applied to describe multilayer adsorption which also includes monolayer adsorption. The linear form of Freundlich equation is:

$$\log q_e = \log K_F + \frac{1}{n}\log C_e \quad (6)$$

where K_F and n are Freundlich isotherm constants and C_e is the equilibrium concentration (mg/L) which relate to sorption capacity and sorption intensity. The intercept and slope of $\log q_e$ against $\log C_e$ plot show the adsorption isotherm constants. The plot of $\log q_e$ vs. $\log C_e$ was performed to evaluate the Freundlich isotherm constants K_F and n (Fig. 8b). The plot of Freundlich isotherm (Fig. 8b) was fitted well with the results with $R^2 > 0.95$ (Table 2). n values of isotherm were 3.36 greater than 1 indicating a high affinity adsorption between adsorbate and adsorbent and also chemisorption [26,39,40]. Both isotherm model results suggested the high adsorption and affinity of nZVI to adsorb Pb^{2+}.

The adsorption capacity of Pb^{2+} by nZVI compared to other reports is shown in Table 3. Based on the literatures there was another report for very high adsorption capacity of Pb on pure nZVI particles as higher than 1,600 mg/L [17]. From Table 3, the comparison showed that Pb^{2+} adsorption capacity of pure nZVI was very high compared with other composited nZVI with other materials. These suggested that the support materials may reduce the reactive power of nZVI due to the decrease of particle surface area. There were several studies reported that the adsorption of lead by nZVI follows two mechanisms which occurred all together. The first mechanism was co-precipitation and adsorption. When the nZVI was added into the acidic spent regeneration waste containing Pb^{2+}, H^+ was consumed and the shell of nZVI was oxidized into oxide which ready for adsorption. The pH of the solution increased to 7–8 so that the iron did not dissolve into the solution. Under the pH more than the point of zero charge, the surface charge of iron oxide shell was deprotonated into negatively charge (FeO^-) resulting in favor for Pb^{2+} adsorption through the combination of coulombic and Lewis acid base interactions and form oxide of Pb^{2+} in the shell (oxide of Fe) of nZVI particle. The second mechanism was the reduction reaction occurred during the oxidation of nZVI shell, electrons release from the reaction directly reduced Pb^{2+} to Pb^0 [17,25,31]. The XANES

Table 3
Pb^{2+} adsorption capacities of pure nZVI compared with other materials

Adsorbent	q_{max} (mg/g)	Reference
Ti(IV) iodovanadate cation exchanger	18.8	[42]
SDS-AZS nano-composite cation exchanger	18.4–21.01	[43]
Fe nanoparticles loaded ash (nFe-A)	30	[44]
Kaolinite-supported nZVI	48	[45]
Kaolin supported nZVI	90	[46]
nZVI supported on *sinegulas* waste	225	[47]
Zeolite-nZVI	806	[27]
Pure nZVI	>1,600	This work and [17]

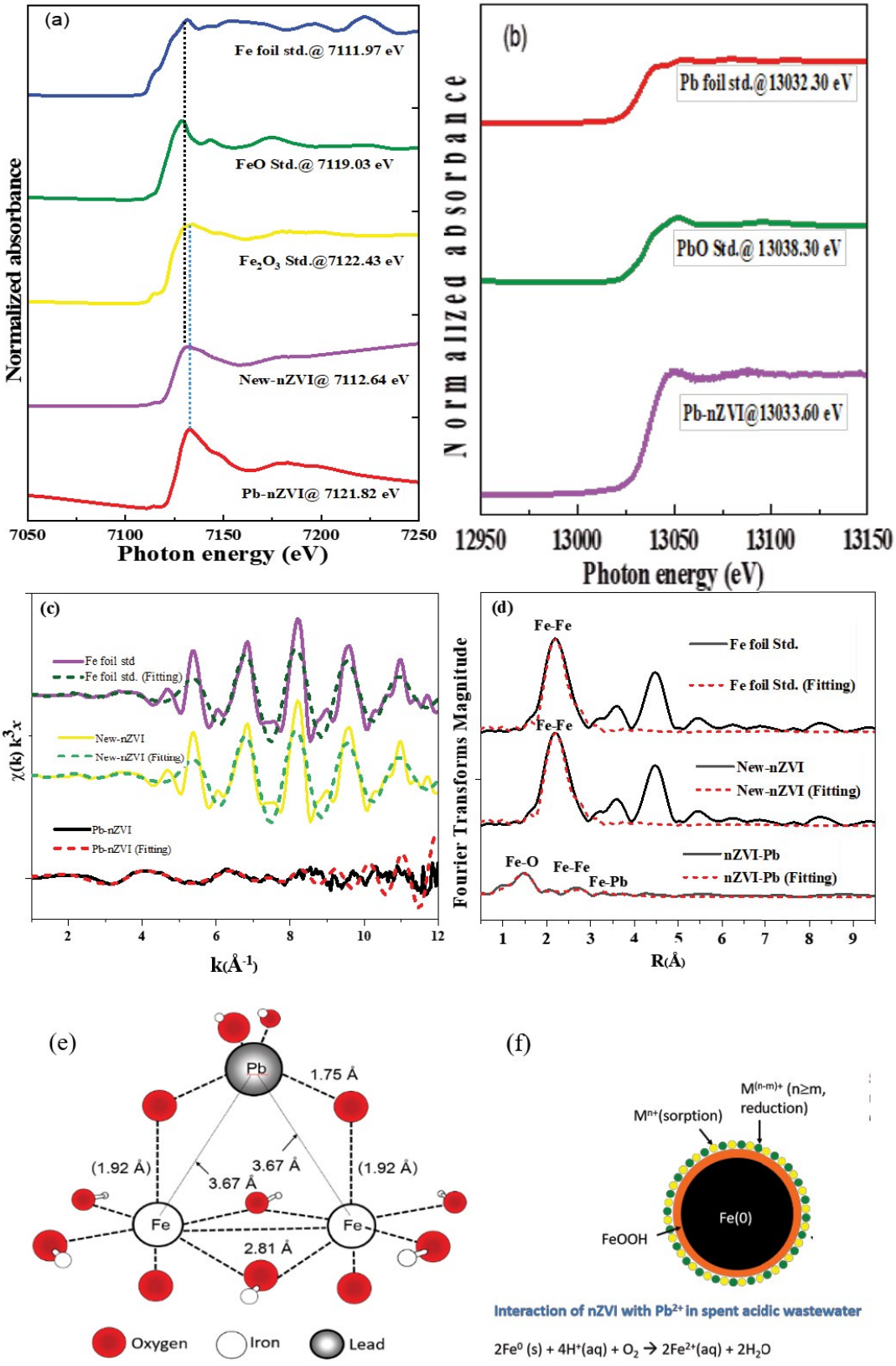

Fig. 9. (a) Normalized XANES of Fe *K*-edge XANES, (b) Pb L_3-edge XANES, (c) Fourier transforms of $k^3 \cdot \chi(k)$ into *R* space, where the dashed lines correspond to the curve-fitting results, (d) $k^3 \cdot \chi(k)$ in the *k* range of 1.0–12.0 $Å^{-1}$, where the dotted lines correspond to the curve-fitting results, (e) proposed Pb adsorption onto the surface of iron oxide through the formation of bidentate inner-sphere complex, and (f) interaction of nZVI with Pb^{2+} in spent acidic wastewater.

characterization techniques will be used to identify the oxidation state of both nZVI and Pb^{2+} before and after reactions.

3.7. XANES and EXAFS analysis for Pb removal at high concentration

The XANES was determined to investigate the oxidation state of the adsorbed atom. The Fe foil, FeO, and Fe_2O_3 were used as reference of Fe *K*-edge XANES. As shown in Fig. 9a, The XANES absorption peak of the new-nZVI sample was similar to those in Fe foil. The nZVI adsorbed Pb (Pb-nZVI) sample was shown absorption edge energy of 7,121.82 eV mixed oxidation state of FeO and Fe_2O_3, which was between the values of FeO and Fe_2O_3, confirming the mixed oxidation state of Fe species. Fig. 9b shows the XANES spectra for Pb L_3-edge of Pb foil and PbO for reference. The nZVI adsorbed Pb(II) (Pb-nZVI) sample was mixed oxidation state between Pb(0) and Pb(II), indicating the Pb(II) was reduced to Pb(0) by nZVI. Thus, the nZVI adsorbed Pb sample is could be oxidized Fe^0 to Fe^{2+} and Fe^{3+} and Pb^{2+} was reduced to Pb^0 by nZVI and adsorption by Fe oxide in the shell of nZVI.

Extended EXAFS spectroscopy measurements were performed to investigate an element-specific technique for characterizing the electronic configurations and local coordination structures of the Fe atom. The Fourier transform of the Fe *K*-edge EXAFS data of the reference sample was identical to that of iron [41]. In comparison, the first and second shell of iron in the Fe foil and new-nZVI sample appears to be at a shorter distance approximately 2.45 and 2.83 Å, respectively. Fig. 9c shows the corresponding $k^3 \cdot \chi(k)$ in the k range of 1.0–12.0 $Å^{-1}$, and Fig. 9d shows the Fourier-transformed k^3-weighted EXAFS oscillations into R space of Fe *K*-edge in Fe reference and nZVI samples. The Pb-nZVI was observed peaks at 1.92, 2.81, and 3.67 Å in Fourier transformed spectra corresponded to Fe–O, Fe–Fe, and Fe-Pb distances, respectively and their corresponding parameters (i.e., coordination shell, bond distances, coordination number-CN, Debye-Waller factors-σ^2) were summarized in Table 4. From previous studies, found the bond distance of Fe-Pb which are in a range of 3.30 Å [19]. The results of EXAFS analysis indicated that the adsorption of Pb^{2+} into nZVI through the formation of bidentate inner-sphere complex. Fig. 9e illustrates a schematic of the proposed mechanism of Pb onto the surface of iron oxide surface with related to the adsorption capacity results, which referred that two atoms of iron can interact with one atom of lead.

4. Conclusion

The results of this work show that nZVI particles have effective adsorption properties for removing lead ion from contaminated wastewater sources. Lead can be immediately removed within an hour with capacity over 1,000 mg-Pb/g-nZVI (1,666 mg-Pb/g-nZVI from Langmuir isotherm). The pseudo-second-order kinetic model is the promising adsorption kinetics to describe the adsorption behavior. This relationship may be used to develop the use of nZVI to remove lead contaminated in water for engineering application in the future. The adsorption mechanism consists of both immediately surface adsorption and IPD until reaching to equilibrium state at low initial concentration. On the other hand, at high concentration of initial Pb^{2+}, the adsorption mechanism is more complex related to the limitation of adsorption surface. However, IPD is also the control mechanism. The Langmuir and the Freundlich isotherm models can be fitted very well, which indicates the applicability of monolayer coverage and chemisorption process of Pb^{2+} adsorbed on nZVI particle surface. SEM image shows the change of the physical body of particles and EDS analysis confirms that Pb^{2+} is adsorbed onto the surface of nZVI particles. XANES and EXAFS analysis results reveal that Pb adsorped by nZVI was mixed oxidation state between Pb(0) and Pb(II), indicating the Pb(II) was reduced to Pb(0) by nZVI and Pb atoms can adsorb onto the surface ferric oxide through the formation of inner-sphere complex with distance between Fe and Pb atoms approximately 3.67 Å. Based on the results, pure nZVI has potential to be an effective adsorption material for treating of high concentration of Pb^{2+} contaminated wastewater.

Acknowledgments

This research is financially supported by National Science and Technology Development Agency, Ministry of Science and Technology, Thailand. The laboratory was supported by Department of Environmental Engineering, King Mongkut's University of Technology Thonburi, the Synchrotron Research Funding from Khon Kaen University,

Table 4
Curve-fitting results of Fe *K*-edge EXAFS, $S_0^2 = 0.959$

Sample	Shell	CN[a]	R (Å)[b]	$\sigma^2 \times 10^{-3}$ (Å)	E_0 (eV)
Fe foil standard	Fe–Fe	7*	2.45 ± 0.01	5.55 ± 0.83	5.50 ± 1.50
	Fe–Fe	7*	2.83 ± 0.01	8.51 ± 1.53	5.50 ± 1.50
New-nZVI	Fe–Fe	7.3 ± 1.1	2.45 ± 0.01	5.79 ± 0.91	5.68 ± 1.61
	Fe–Fe	8.2 ± 2.3	2.83 ± 0.01	9.96 ± 2.86	5.68 ± 1.61
nZVI–Pb(II)	Fe–O	5.6 ± 2.2	1.92 ± 0.03	14.33 ± 6.42	–4.14 ± 3.66
	Fe–Fe	3.3 ± 1.1	2.81 ± 0.08	10.74 ± 34.60	–4.14 ± 3.66
	Fe–Pb	2.2 ± 1.0	3.67 ± 0.08	1.88 ± 20.48	–4.14 ± 3.66

CN[a], coordination number; R^b, bond distance; σ^{2c}, Debye–Waller factor.
*Parameters marked with an asterisk were kept fixed.

and Research center for Environmental and Hazardous Substance Management, Khon Kaen University, Khon Kaen, Thailand. These XAS experiments were performed on Synchrotron Light Research Institute (SLRI), Thailand. We are grateful to staff of BL5.2 and BL8 at SLRI for providing assistance in using beamline BL5.2 and BL8.

References

[1] L. Li, M. Fan, R.C. Brown, J. Van Leeuwen, J. Wang, W. Wang, Y. Song, P. Zhang, Synthesis, properties, and environmental applications of nanoscale iron-based materials: a review, Crit. Rev. Environ. Sci. Technol., 36 (2006) 405–431.
[2] X.-q. Li, D.W. Elliott, W.-x. Zhang, Zero-valent iron nanoparticles for abatement of environmental pollutants: materials and engineering aspects, Crit. Rev. Solid State Mater. Sci., 31 (2006) 111–122.
[3] C.-B. Wang, W.-x. Zhang, Synthesizing nanoscale iron particles for rapid and complete dechlorination of TCE and PCBs, Environ. Sci. Technol., 31 (1997) 2154–2156.
[4] W.-x. Zhang, Nanoscale iron particles for environmental remediation: an overview, J. Nanopart. Res., 5 (2003) 323–332.
[5] J. Cao, D. Elliott, W.-x. Zhang, Perchlorate reduction by nanoscale iron particles, J. Nanopart. Res., 7 (2005) 499–506.
[6] W. Elliott Daniel, H.-L. Lien, W.-X. Zhang, Degradation of lindane by zero-valent iron nanoparticles, J. Environ. Eng., 135 (2009) 317–324.
[7] S.R. Kanel, B. Manning, L. Charlet, H. Choi, Removal of arsenic(III) from groundwater by nanoscale zero-valent iron, Environ. Sci. Technol., 39 (2005) 1291–1298.
[8] H.-L. Lien, W.-X. Zhang, Nanoscale Pd/Fe bimetallic particles: catalytic effects of palladium on hydrodechlorination, Appl. Catal., B, 77 (2007) 110–116.
[9] G.V. Lowry, K.M. Johnson, Congener-specific dechlorination of dissolved PCBs by microscale and nanoscale zerovalent iron in a water/methanol solution, Environ. Sci. Technol., 38 (2004) 5208–5216.
[10] S.M. Ponder, J.G. Darab, T.E. Mallouk, Remediation of Cr(VI) and Pb(II) aqueous solutions using supported, nanoscale zero-valent iron, Environ. Sci. Technol., 34 (2000) 2564–2569.
[11] H. Song, E.R. Carraway, Reduction of chlorinated ethanes by nanosized zero-valent iron: kinetics, pathways, and effects of reaction conditions, Environ. Sci. Technol., 39 (2005) 6237–6245.
[12] C. Su, R.W. Puls, Nitrate reduction by zerovalent iron: effects of formate, oxalate, citrate, chloride, sulfate, borate, and phosphate, Environ. Sci. Technol., 38 (2004) 2715–2720.
[13] Z. Xiong, D. Zhao, G. Pan, Rapid and complete destruction of perchlorate in water and ion-exchange brine using stabilized zero-valent iron nanoparticles, Water Res., 41 (2007) 3497–3505.
[14] R. National Center for Environmental, U.S. EPA Workshop on Nanotechnology for Site Remediation, U.S. Department of Commerce, Washington, DC, October 20–21, 2005, U.S. Environmental Protection Agency, Washington, DC, 2005.
[15] N.C. Mueller, J. Braun, J. Bruns, M. Černík, P. Rissing, D. Rickerby, B. Nowack, Application of nanoscale zero valent iron (NZVI) for groundwater remediation in Europe, Environ. Sci. Pollut. Res., 19 (2012) 550–558.
[16] Y. Xi, M. Mallavarapu, R. Naidu, Reduction and adsorption of Pb^{2+} in aqueous solution by nano-zero-valent iron—a SEM, TEM and XPS study, Mater. Res. Bull., 45 (2010) 1361–1367.
[17] Y. Zhang, Y. Su, X. Zhou, C. Dai, A.A. Keller, A new insight on the core–shell structure of zerovalent iron nanoparticles and its application for Pb(II) sequestration, J. Hazard. Mater., 263 (2013) 685–693.
[18] H. Needleman, Lead poisoning, Annu. Rev. Med., 55 (2004) 209–222.
[19] N. Chanthapon, S. Sarkar, P. Kidkhunthod, S. Padungthon, Lead removal by a reusable gel cation exchange resin containing nano-scale zero valent iron, Chem. Eng. J., 331 (2018) 545–555.
[20] N. Rahman, U. Haseen, M. Rashid, Synthesis and characterization of polyacrylamide zirconium(IV) iodate ion-exchanger: its application for selective removal of lead(II) from wastewater, Arabian J. Chem., 10 (2017) S1765–S1773.
[21] X.-q. Li, W.-x. Zhang, Iron nanoparticles: the core−shell structure and unique properties for Ni(II) sequestration, Langmuir, 22 (2006) 4638–4642.
[22] M.A.V. Ramos, W. Yan, X.-q. Li, B.E. Koel, W.-x. Zhang, Simultaneous oxidation and reduction of arsenic by zero-valent iron nanoparticles: understanding the significance of the core−shell structure, J. Phys. Chem. C, 113 (2009) 14591–14594.
[23] O. Çelebi, Ç. Üzüm, T. Shahwan, H.N. Erten, A radiotracer study of the adsorption behavior of aqueous Ba^{2+} ions on nanoparticles of zero-valent iron, J. Hazard. Mater., 148 (2007) 761–767.
[24] Ç. Üzüm, T. Shahwan, A.E. Eroğlu, K.R. Hallam, T.B. Scott, I. Lieberwirth, Synthesis and characterization of kaolinite-supported zero-valent iron nanoparticles and their application for the removal of aqueous Cu^{2+} and Co^{2+} ions, Appl. Clay Sci., 43 (2009) 172–181.
[25] W. Yan, A.A. Herzing, C.J. Kiely, W.-x. Zhang, Nanoscale zero-valent iron (nZVI): aspects of the core-shell structure and reactions with inorganic species in water, J. Contam. Hydrol., 118 (2010) 96–104.
[26] H.K. Boparai, M. Joseph, D.M. O'Carroll, Kinetics and thermodynamics of cadmium ion removal by adsorption onto nano zerovalent iron particles, J. Hazard. Mater., 186 (2011) 458–465.
[27] S.A. Kim, S. Kamala-Kannan, K.-J. Lee, Y.-J. Park, P.J. Shea, W.-H. Lee, H.-M. Kim, B.-T. Oh, Removal of Pb(II) from aqueous solution by a zeolite–nanoscale zero-valent iron composite, Chem. Eng. J., 217 (2013) 54–60.
[28] Y.-P. Sun, X.-q. Li, J. Cao, W.-x. Zhang, H.P. Wang, Characterization of zero-valent iron nanoparticles, Adv. Colloid Interface Sci., 120 (2006) 47–56.
[29] Y.-P. Sun, X.-Q. Li, W.-X. Zhang, H.P. Wang, A method for the preparation of stable dispersion of zero-valent iron nanoparticles, Colloids Surf., A, 308 (2007) 60–66.
[30] J. Goldstein, D.E. Newbury, D.C. Joy, C.E. Lyman, P. Echlin, E. Lifshin, L. Sawyer, J.R. Michael, Scanning electron microscopy and X-ray microanalysis, Scanning, 27 (2003) 215–216.
[31] X.-q. Li, W.-x. Zhang, Sequestration of metal cations with zerovalent iron nanoparticles–a study with high resolution X-ray photoelectron spectroscopy (HR-XPS), J. Phys. Chem. C, 111 (2007) 6939–6946.
[32] S. Azizian, Kinetic models of sorption: a theoretical analysis, J. Colloid Interface Sci., 276 (2004) 47–52.
[33] Y.-S. Ho, Review of second-order models for adsorption systems, J. Hazard. Mater., 136 (2006) 681–689.
[34] D. Kavitha, C. Namasivayam, Experimental and kinetic studies on methylene blue adsorption by coir pith carbon, Bioresour. Technol., 98 (2007) 14–21.
[35] S.I.H. Taqvi, S.M. Hasany, M.I. Bhanger, Sorption profile of Cd(II) ions onto beach sand from aqueous solutions, J. Hazard. Mater., 141 (2007) 37–44.
[36] F.-C. Wu, R.-L. Tseng, R.-S. Juang, Initial behavior of intraparticle diffusion model used in the description of adsorption kinetics, Chem. Eng. J., 153 (2009) 1–8.
[37] M. Barkat, D. Nibou, S. Chegrouche, A. Mellah, Kinetics and thermodynamics studies of chromium(VI) ions adsorption onto activated carbon from aqueous solutions, Chem. Eng. Process. Process Intensif., 48 (2009) 38–47.
[38] P. Chingombe, B. Saha, R.J. Wakeman, Sorption of atrazine on conventional and surface modified activated carbons, J. Colloid Interface Sci., 302 (2006) 408–416.
[39] J.-Q. Jiang, C. Cooper, S. Ouki, Comparison of modified montmorillonite adsorbents: part I: preparation, characterization and phenol adsorption, Chemosphere, 47 (2002) 711–716.
[40] I. Mironyuk, T. Tatarchuk, M. Naushad, H. Vasylyeva, I. Mykytyn, Highly efficient adsorption of strontium ions by carbonated mesoporous TiO_2, J. Mol. Liq., 285 (2019) 742–753.
[41] W. Yan, R. Vasic, A.I. Frenkel, B.E. Koel, Intraparticle reduction of arsenite (As(III)) by nanoscale zerovalent iron (nZVI) investigated with *in situ* X-ray absorption spectroscopy, Environ. Sci. Technol., 46 (2012) 7018–7026.

[42] M. Naushad, Z.A. Alothman, M.R. Awual, M.M. Alam, G.E. Eldesoky, Adsorption kinetics, isotherms, and thermodynamic studies for the adsorption of Pb^{2+} and Hg^{2+} metal ions from aqueous medium using Ti(IV) iodovanadate cation exchanger, Ionics, 21 (2015) 2237–2245.

[43] M. Naushad, Surfactant assisted nano-composite cation exchanger: development, characterization and applications for the removal of toxic Pb^{2+} from aqueous medium, Chem. Eng. J., 235 (2014) 100–108.

[44] M. Ghasemi, M. Ghasemi, N. Ghasemi, Y. Khosravi-Fard, Adsorption of Pb(II) from aqueous solution using new adsorbents prepared from agricultural waste: adsorption isotherm and kinetic studies, J. Ind. Eng. Chem., 20 (2014) 2193–2199.

[45] X. Zhang, S. Lin, Z. Chen, M. Megharaj, R. Naidu, Kaolinite-supported nanoscale zero-valent iron for removal of Pb^{2+} from aqueous solution: reactivity, characterization and mechanism, Water Res., 45 (2011) 3481–3488.

[46] X. Zhang, S. Lin, X.-Q. Lu, Z.-l. Chen, Removal of Pb(II) from water using synthesized kaolin supported nanoscale zero-valent iron, Chem. Eng. J., 163 (2010) 243–248.

[47] M. Arshadi, M. Soleymanzadeh, J.W. Salvacion, F. SalimiVahid, Nanoscale zero-valent iron (NZVI) supported on sineguelas waste for Pb(II) removal from aqueous solution: kinetics, thermodynamic and mechanism, J. Colloid Interface Sci., 426 (2014) 241–251.